Chapter 2
Passive Load-Pull Systems

In general, a passive load-pull system is built around a passive tuner. The tuner is used in combination with peripheral equipment and components, such as a vector network analyzer (VNA), signal generators, power meters, bias tees, isolators, for achieving the load-pull functionality. Primarily two types of passive tuners, namely the electromechanical tuner (EMT) and the electronic tuner (ETS), are employed in load-pull systems. It is imperative to understand the limitations of both these tuners so that the best solution can be employed for any specified application. The initial sections of this chapter are focused on the explanation and comparison of EMT and ETS based passive load-pull systems.

The major challenge in setting up a passive load-pull setup involves calibration, which is carried out to remove errors arising from mismatches, dispersions and imperfections in the cables and system components. A second aspect of calibration involves shifting of the measurement planes, considering that the actual measurement takes place away from the device under test (DUT) ports. Later sections of this chapter address the calibration aspect in detail.

2.1 Introduction

An impedance tuner is the main engine of any passive load-pull system [1–4]. The tuner is placed between the DUT and power meter, as shown in Fig. 2.1, for the search of optimal matching conditions for given targeted performance. The synthesis of optimal impedance involves changing of the tuner setting and then measuring subsequently the output power, P_{out}, using the power meter. The optimal impedance synthesized by the impedance tuner corresponds to the maximum reading of P_{out} by the power meter, according to the maximum power transfer theorem [5]. A separate power meter measures the power injected, P_{in}, by the source at the input of DUT.

Overall, setting of the impedance tuner directly provides the matching reflection coefficient, as given in Eq. (2.1), while readings of the power meters at the input and output relates the incident and reflected traveling waves, as given in Eqs. (2.2) and (2.3), at the respective DUT ports.

F.M. Ghannouchi, M.S. Hashmi, *Load-Pull Techniques with Applications to Power Amplifier Design*, Springer Series in Advanced Microelectronics 32
DOI 10.1007/978-94-007-4461-5_2, © Springer Science+Business Media Dordrecht 2013

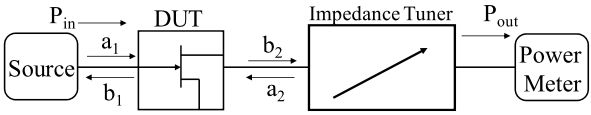

Fig. 2.1 Typical representation of a passive load-pull system

$$\Gamma_{out} = \frac{a_2}{b_2} \tag{2.1}$$

$$P_{in} = |a_1|^2 - |b_1|^2 = |a_1|^2\left(1 - |\Gamma_{in}|^2\right) \tag{2.2}$$

$$P_{out} = |b_2|^2 - |a_2|^2 = |b_2|^2\left(1 - |\Gamma_{out}|^2\right) \tag{2.3}$$

where, Γ_{out} and Γ_{in} are the reflection coefficients at the output and input ports of the DUT, respectively; and, a and b with subscripts represent the incident and reflected waves at the respective ports.

The optimal values of Eqs. (2.1), (2.2), (2.3) enable the determination of design parameters such as gain, efficiency and power-added efficiency (PAE). The determination of the optimal values and, subsequently, the design parameters is an iterative process and requires numerous changes in the configuration of the load-pull tuner.

2.2 Passive Load-Pull System

A passive load-pull system typically employs either electromechanical tuners (EMTs) that rely on horizontal and vertical movement of probes along a transmission line [6] or electronic tuners (ETSs), which rely on the appropriate electronic circuits with electronically changing matching properties [7]. EMTs are stub, slug or slide screw type [8, 9], whereas ETSs are mostly solid state and employ PIN diodes [10, 11].

2.2.1 Electromechanical Tuner (EMT)

These tuners allow precise positioning of probes/stubs/slugs in a slotted transmission line, in order to generate repeatable complex microwave reflection factors. Movement of the probes changes the impedance by changing the parallel susceptance. The probes are called mismatched elements and introduce mismatch through their movement in the horizontal and vertical directions. The movement of a probe in the vertical direction alters mainly the magnitude of the mismatch, while its movement in the horizontal direction alters mainly the phase of the mismatch.

A pictorial presentation of working principle of single-stub EMT is depicted in Fig. 2.2 [12]. In Fig. 2.2(a), the stub is outside the electric fields of the traveling wave propagating in the central conductor (transmission line) and, therefore, does not affect the impedance at the reference plane (usually set at 50 Ω). However, as soon as the probe moves vertically downward towards the central conductor (transmission line) the magnitude of the reflection factor at the reference plane increases, as can

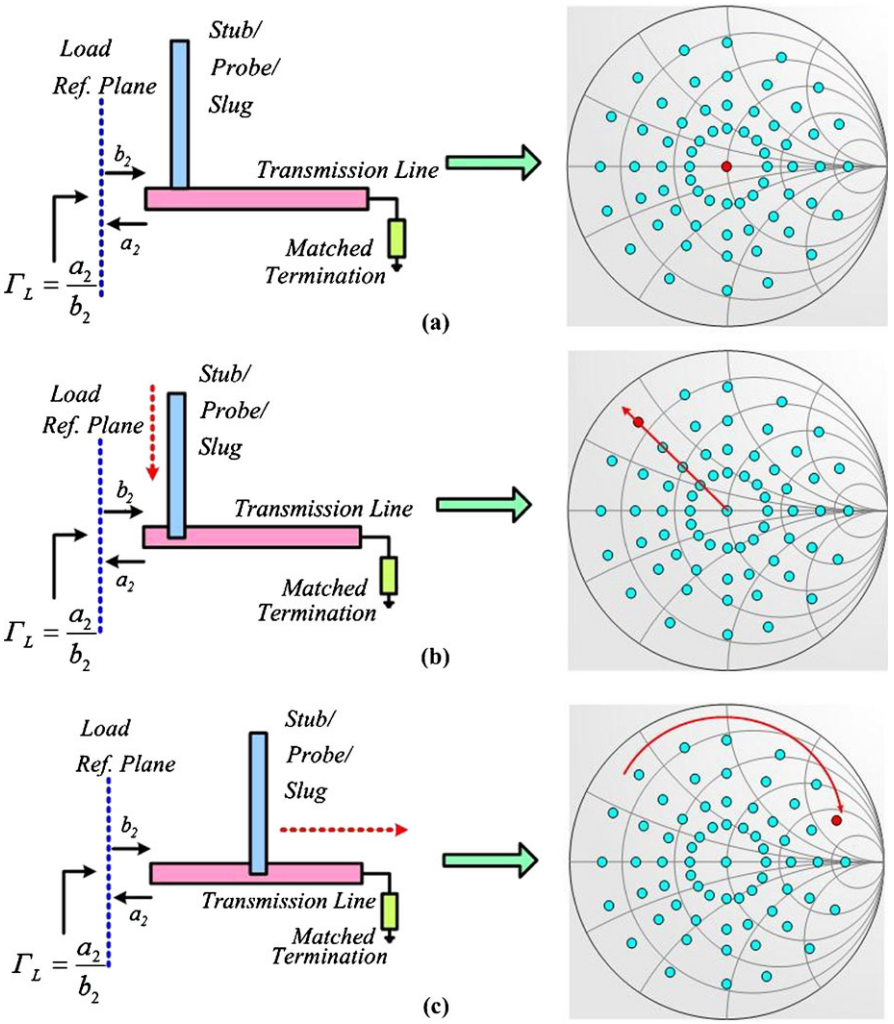

Fig. 2.2 (**a**) A generic representation of an EMT in a matched state, (**b**) the movement of a stub/probe/slug in the vertical direction changes the magnitude of the reflection factor, (**c**) the movement of a stub/probe/slug in the horizontal direction alters the phase of the reflection factor [12]; © IEEE 2011

be seen in Fig. 2.2(b). The movement of the probe in the horizontal direction along the central conductor varies the phase of the reflection coefficient, as evident in Fig. 2.2(c).

In principle, in any EMT, the magnitude of the impedance mismatch at the reference plane is determined by the probe position (depth); and, the phase of the impedance mismatch at the reference plane is determined by the carriage position across the length of the tuner length. An EMT is considered good if the resolution

Fig. 2.3 A single probe tuner, photo © Focus Microwaves Inc.

of the movements of the stub/slug/probe in the horizontal and vertical directions is incrementally small in range of tens of microns [13]. A good EMT ensures that the desired reflection coefficient can be synthesized on a dense grid. An example of a commercial EMT (in this case, a single probe tuner) is given in Fig. 2.3.

The slide screw type of EMT consists of a 50 Ω coax- or slab-line with a probe with a nominal minimum length of $\lambda/4$ at its lowest frequency of operation and has two degrees of freedom [14, 15]. One movement is up and down towards the center conductor. This way the probe forms an adjustable shunt discontinuity with the 50 Ω transmission line. The other movement is the traveling of the probe along the 50 Ω mainline.

In stub tuners, two or more parallel sliding shorts (stubs) are placed on a 50 Ω line. When one is placed at the DUT reference plane and another $\lambda/8$ away from it, they independently control the real and imaginary parts of the admittance [6]. For a reflection factor (Γ_L) setting of 0, each stub has to be set to precisely $n\lambda/8$. A very high voltage standing wave ratio (VSWR) can be reached with a stub tuner.

The slug tuner is a construction with a 50 Ω coax- or slab-line, where two movable slugs can slide over the center conductor. The slug reduces the characteristic impedance locally to typically 10–15 Ω, while an electrical length of $\lambda/8$ for the transmission line gives maximum tuning range. In slug tuners, setting maximum $\Gamma_L(|\Gamma_L|)$ is easier, and losses tend to be constant over the tuning range, compared to other EMT types [6].

Overall, in a coaxial environment, the frequencies at which EMT can be used are around 200 MHz to 50 GHz in different multi-octave bands and tuner types. EMTs that use waveguides cover standard WR bands from 26.5 to 110 GHz [13].

In any automatic load-pull system based around an EMT, the movements of the probes in the horizontal and vertical directions are achieved through stepper motors; and, the actual positioning of the probe are monitored and controlled by timing belts. The use of timing belt to control axis positioning minimizes the vibrations translated from the stepper motors to the axis and then the probes [3] and, thus, makes these systems useful for on-wafer applications. In most cases, EMTs use the same vertical anti-backlash mechanism with a resolution of 0.75 or 1.5 μm per motor step; and,

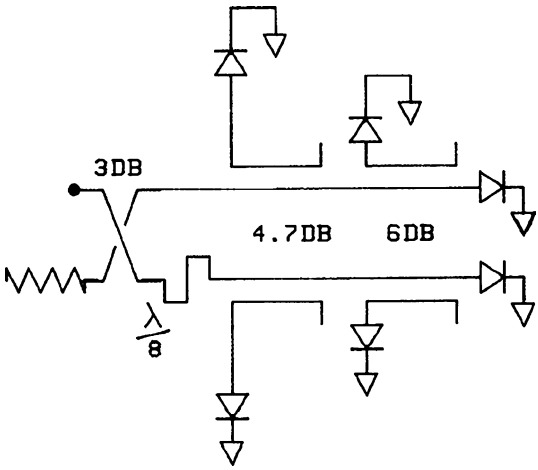

Fig. 2.4 A generic diagram of a 6-diode based electronic tuner [10], © IEEE 1982

the horizontal step size varies between 1.25 and 25 μm, depending on the frequency of operation, in order to obtain an optimal tuning speed/resolution ratio [13].

2.2.2 Electronic Tuner (ETS)

An ETS is an electronic circuit with the ability to electronically change matching properties. These electronic circuits can be based on either varactor or PIN diodes. The latter is more common for load-pull applications, due to the ability to handle higher power compared to varactor-based ETS. The diode-based ETS synthesize reflection coefficient by varying the impedance state of a number of PIN diodes connected in parallel and placed in a precise manner along a transmission line, an example of which is shown in Fig. 2.4.

In such a configuration, each diode is capable of generating a continuous discontinuity as a spoke of a wheel of increasing $|\Gamma_L|$, while other diodes can subsequently change the angle of Γ_L discretely. The ETS in Fig. 2.4 consists of directional couplers, six PIN diodes, and external loads. This six-diode ETS can produce a total of sixty-four (2^6) impedance states, corresponding to two states of each diode independently. Depending on the design, the diode impedance state can be varied continuously or toggled discretely between on and off states [10].

Essentially, a single ETS is limited in tuning resolution; therefore, a number of ETSs are cascaded together for applications requiring higher tuning resolution. The cascaded configuration is transparent to the user and, therefore, behaves as one tuner unit. Passive ETSs are generally quite lossy and, therefore, can usually achieve VSWRs up to 10 [7]. However, their miniature size and light weight make them appropriate for on-wafer measurements.

Table 2.1 Comparison between ETS and EMT [16]

Characteristics	ETS	EMT
Reflection Factor, Γ	Noise: O Load Pull: -	++
Number of Impedances	O	++
Insertion Loss	-	+/++
Tuning Resolution	Noise: O Load Pull: –	++
Maximum Power	O / - / – Depending on DUT	++
Frequency Bandwidth	O	++
Spurious Oscillations	O / -	++
On Wafer Operation	++	O
Tuner Size	++	On Wafer: - Test Fixture: ++
Tuner Speed	++	-
Test Total Speed	+	+
Tuner Linearity	O / - Depending on DUT	++
DSB Noise Measurement	–	+
Temperature Drift	-	++

Legend: ++ Excellent; + Good; O Acceptable; - Poor; – Unacceptable for certain tasks

2.2.3 ETS and EMT Comparisons

Load-pull systems are employed in diverse applications, such as the design of power amplifiers and oscillators and noise measurements,. As a consequence it is imperative to understand the features and limitations of ETSs and EMTs. Table 2.1 provides a comparison between EMT and ETS based on the most common load-pull parameters and applications [16].

ETSs consist of sets of PIN diodes, mounted in microstrip circuits, having only two states, i.e., on and off. Due to the physical distribution along microstrip lines, ETSs generate irregular shapes of reflection factors with values up to 0.8 over a limited frequency range [16]. An EMT can generate a reflection factor (Γ) of 0.75 in standard form and up to 0.92 in a pre-matched or cascaded state from low frequencies up to millimeter waves [17, 18].

ETSs are faster and can change states from impedance to impedance within milliseconds, whereas EMTs take at least a few seconds to tune from one state to another. However, it should be noted that ETS can save only around 10 % of the measurement time compared to that of EMT during the complete load-pull measurements, due to the time needed to read the instrumental setup via general purpose interface bus (GPIB) [16]. ETSs are also miniature, compact and substantially

smaller compared to EMTs, making the ETS more suitable for applications prone to mechanical vibrations, such as on-wafer device characterization and measurement.

The insertion loss of an ETS at the operating reflection factor is very high, due to lossy microstrip lines. This requires high-power driver amplifiers at the source side of the setup, which in turn raises the question of linearity of the PIN diodes and the temperature drift in the ETS. An ETS operating loss of 12 dB at $\Gamma = 0.8$ is a common observable fact, this results in raising the cost of the setup considerably, whereas an EMT has only a few tenths of a dB at this Γ level [16].

The ETS has unpredictable impedance behavior at low frequencies, whereas the EMT is low pass and presents 50 Ω to the DUT. The ETS behavior is a high risk factor for uncontrollable spurious oscillations outside the test band. An EMT does not create parasitic oscillations, in principle, at low frequencies.

The tuning repeatability accuracy of ETS is around −70 to −80 dB, and the tuning accuracy of a modern EMT is around −60 dB. However, for accurate noise and load-pull measurements, tuning accuracies of −40 dB are sufficient [16].

In terms of tuning resolution, EMTs possess high resolution, thereby allowing fine-tuning to the optimal performance of the DUT; whereas an ETS exhibits irregular impedance patterns with the points jumping unpredictably when the diodes are switched on and off and, therefore, is not able to fine-tune to the optimal performance of the DUT. In noise measurements, the unpredictable jumping of impedance states for small frequency changes prohibits the use of ETSs in double sideband setups. This necessitates either YIG (yttrium iron garnet) filters or other expensive single sideband noise receivers. They do not allow direct measurement of the minimum noise figure, NF_{min}, by tuning to the optimal reflection factor Γ_{opt}; whereas EMT allows fine-tuning and can, therefore, directly measure NF_{min}.

ETS is favored for on-wafer applications; however, EMT has been used in on-wafer applications below 0.8 GHz, after performing appropriate vibration tests [3].

2.3 Load-Pull Measurement

The load-pull measurement procedure primarily involves the following three steps:

- Assembly of the system components to establish a load-pull measurement setup.
- Calibration of the load-pull measurement setup for correction of errors arising from imperfect system components, dispersions, and mismatches. Calibration for setting the appropriate calibrated reference planes.
- Measurement of relevant data at the calibrated reference planes and then the de-embedding of these data, in order to refer them to the device planes so that the behavior of the DUT can be accurately predicted.

It is imperative to understand the typical setup of a load-pull system, as shown in Fig. 2.5, before getting into the details. As depicted, a standard load-pull system consists of various equipments, such as a directional coupler, impedance tuners, power meters, and a computer for automating and controlling the overall measurement process.

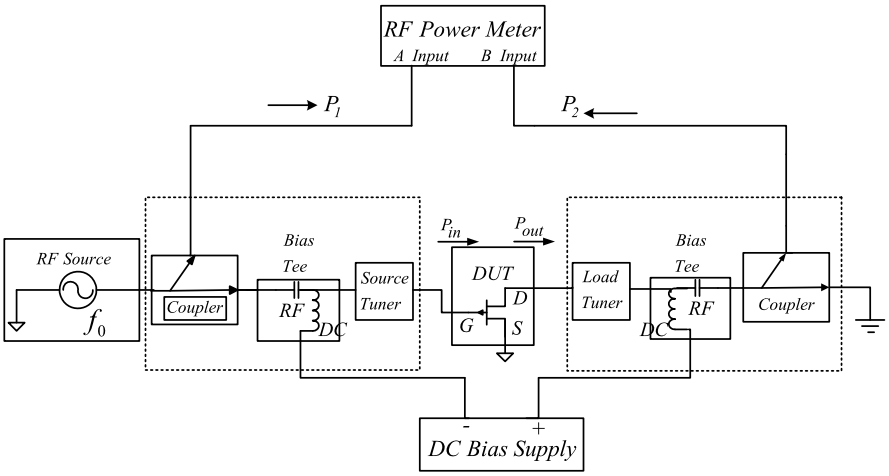

Fig. 2.5 Block diagram of a typical setup that depicts standard components required for carrying out automated load-pull measurements

In the block diagram of Fig. 2.5, the tuners are shown to be close to the DUT ports, ensuring that maximum possible reflection coefficients synthesized by the tuners are directly seen by the DUTs. However, this is a non-real time setup, as all variables must be fixed a priori and then de-embedding procedures must then be applied before measurements are made [19, 20]. Such systems are slow in terms of speeds as compared to real-time load-pull systems [21–24].

In real-time systems, the incident and reflected waves are directly collected from the DUT ports; thus, the measurements are instantaneous with every change in the DUT operating conditions [22–24]. Nonetheless, a non-real-time passive load-pull system is frequently used to utilize maximum synthesizable reflection coefficients from passive tuners [25]. However, with the advancements in passive tuner technologies [9, 18], real-time passive load-pull systems are also possible and will obviously provide better performance in terms of speed, accuracy, flexibility, ease and deployment of the type of tuners.

2.3.1 Load-Pull Setup

Essentially, a complete load-pull measurement setup consists of at least two fundamental tuners (one each at the output and input of the DUT), one signal source, a test fixture or probe station, two power meters or a dual channel power meter, a power supply, a spectrum analyzer, an RF test set (including bias tees, cables, attenuators, couplers, power combiners and dividers), and access to a vector network analyzer (VNA). A generic block diagram of a real-time passive load-pull measurement setup is given in Fig. 2.6 [26].

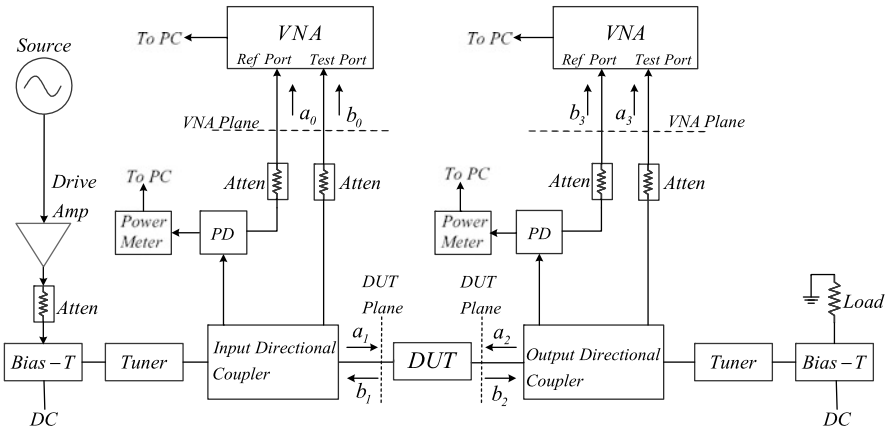

Fig. 2.6 Generic block diagram of a real-time passive load-pull setup [26], © IEEE 1984

The DUT is fed from a high-power microwave source, and its source and load impedances are controlled by adjustable impedance tuners at the input and output. If the DUT is an oscillator, only the output part of the system is needed. Uncorrected large-signal reflection coefficients at the input and output of the DUT are monitored using dual directional couplers and RF network analyzers. Attenuators ensure that the signal levels at the inputs of the harmonic frequency converters are within the safe operating range. If only one network analyzer is available, coaxial switches can be used to connect it back and forth between the input and output circuits.

The power meters are used for the monitoring of the uncorrected power incident on the input port of the DUT and the uncorrected power generated at the output port of the DUT. Only one power meter at each port is required, because the reflection coefficients generated by the tuners are known [27], given that the tuners are pre-characterized using tuner calibration techniques [28–32]. The pre-characterization of tuners ensures that all the imperfections associated with the stub movement in the impedance tuners, central conductor of the tuners and the connectors at the tuner ports are compensated. This step also helps in speeding up the overall measurement, as it enables synthesis of the required reflection coefficient using interpolation instead of multiple actual movements of stubs in the horizontal and vertical directions [13].

The power dividers create reference signals for the respective network analyzers. In principle, in an alternate configuration, the power divider and power meter can be connected to other coupled ports of the respective directional couplers. However, such a configuration results into reduced accuracy in the measurements for the condition when the reflection coefficients at the DUT ports are close to zero and giving very small power meter readings [26, 27].

An interfacing computer (not shown in the figure) is used for controlling the instrument and acquiring and processing the measured data, and for error correction.

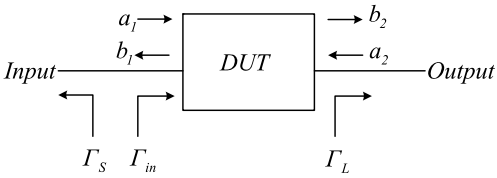

Fig. 2.7 Power waves and the reflection coefficients of interest at the DUT reference planes [26], © IEEE 1984

2.3.2 System Calibration

The main objective behind the load-pull characterization of DUTs is the accurate prediction of device performance under realistic conditions, but the errors due to imperfect system components, such as inherent directivity, mismatch and cross-coupling errors associated with the network analyzer, cause uncertainty in the reflection coefficients and RF power at the specified reference planes, thereby defeating the primary objective.

It is, therefore, extremely important to calibrate the load-pull setup, in order to accurately set and measure the reflection coefficients and, hence, the design parameters, such as PAE, drain efficiency, and gain. The calibration, in principle, serves a dual purpose, by removing the systematic errors arising from imperfections and system components, as well as by shifting the reference plane from the network analyzer measuring planes to the DUT reference planes. In essence, after calibration, the system performs three functionalities, which are critical for achieving accurate load-pull measurement results and can be summarized as:

- Setting a particular impedance value (reflection coefficients).
- Measuring the load reflection coefficients (impedances).
- Measuring the required device performance at the particular impedance.

In practical load-pull measurements, the input and output powers, P_{in} and P_{out}, at the DUT plane, as shown in Fig. 2.7, are given by:

$$P_{in} = |a_1|^2 - |b_1|^2 = |a_1|^2\left(1 - |\Gamma_{in}|^2\right) \tag{2.4}$$

$$P_{out} = |b_2|^2 - |a_2|^2 = |b_2|^2\left(1 - |\Gamma_L|^2\right) \tag{2.5}$$

where Γ_{in} and Γ_L are the reflection coefficients at the input and port of the DUT and the load seen by the DUT, respectively. The traveling waves a_1, b_1, a_2 and b_2 are the incident and reflected waves at the DUT ports as shown in Fig. 2.7.

During load-pull measurement, the impedance tuners set the desired reflection coefficients, whereas the vector network analyzers (VNAs) and power meters in Fig. 2.6 give direct (but uncorrected) measurements of Γ_{in}, Γ_L, $|a_1|^2$ and $|b_2|^2$. The errors introduced by the VNA and the hardware configuration in the measured reflection coefficients significantly affect the accuracy in the measurements of input and output RF power. The accuracy in the measured reflection coefficients and, hence, the RF power is limited, due to the inherent directivity, mismatch, and cross-coupling errors associated with the network analyzer components. These errors impact the performance of the load-pull setup and, in turn, put a question mark on the reliability of the measured data.

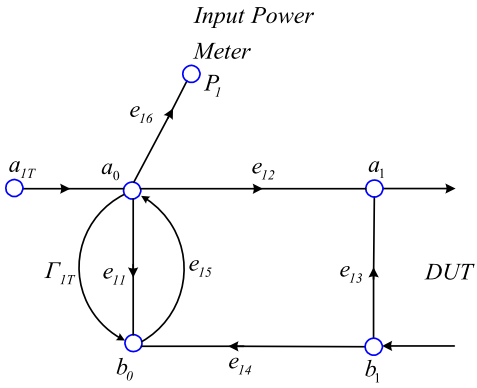

Fig. 2.8 Signal flow error model for the input port incorporating the imperfections contributed by directional coupler, power meter and network analyzer [26], © IEEE 1984

For example, unknown tuner losses add uncertainty in the measured data, if the output power meter is farther from the DUT [1, 33], with tuner losses as large as several decibels [34]. On the other hand, finite coupler directivity and connector mismatches can result in significant errors in the measured RF power in systems where the RF power levels are determined using directional couplers at the input and/or output of the DUT [35, 36]. With 25 dB directivity, errors in the measured power can be as large as 1 dB [26]; and, these errors significantly affect the measurement data, if the VSWR in the directional coupler is high.

Error correction in the measurement can be carried out using the error flow model of the complete measurement system given in Fig. 2.6. The respective error flow models of the input and output ports (as given in Figs. 2.8 and 2.9) incorporate all the errors, such as the finite coupler directivity, connector mismatches, and cross-coupling between the reference and VNA's measuring ports. The models have been simplified using the flow graph reduction technique [5]. The major assumption considered in this simplification is that the reflection coefficients of the power meter sensor heads and the reference and VNA inputs are constant and independent of RF power level. These models form the basis of a unified approach to the vector error correction of RF power and reflection coefficient measurements. These error models are analogous to the error models commonly used for error correction in VNA systems [37], but include some additional terms.

In the error flow model of the input side shown in Fig. 2.8, a_{1T} represents the input signal from the high-power microwave source, Γ_{1T} is the reflection coefficient presented to the input directional coupler by the input tuner, e_{16} represents coupling to the input power meter, and e_{11} represents directivity errors in the reference channel of the input network analyzer. The term e_{13} represents the source mismatch, $e_{12}e_{14}$ denotes the transmission tracking, and e_{15} indicates the error occurring in the measuring port of the VNA. The incident and reflected traveling waves at the input VNA ports are a_0 and b_0, whereas the actual incident and reflected traveling waves at the input ports of DUT are represented by a_1 and b_1, respectively. The VNA measures the uncorrected reflection coefficient, Γ_{in}^{U}, as given in Eq. (2.6):

$$\Gamma_{in}^{U} = \frac{b_0}{a_0} \tag{2.6}$$

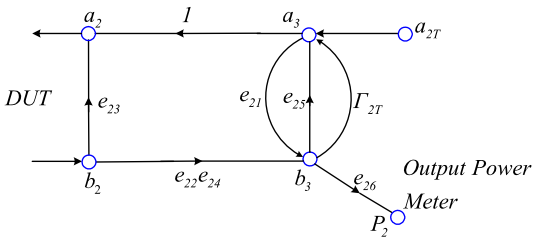

Fig. 2.9 Signal flow error model for the output port incorporating the imperfections contributed by directional coupler, power meter and network analyzer [26], © IEEE 1984

The quantity of interest is, however, the input reflection coefficient, Γ_{in}, expressed in Eq. (2.7), which relates the error terms and the input uncorrected reflection coefficient measured at the input VNA plane in Fig. 2.7.

$$\Gamma_{in} = \frac{b_1}{a_1} = \frac{\Gamma_{in}^U - e_{11}}{e_{12}e_{14} - e_{11}e_{13} + e_{13}\Gamma_{in}^U} \tag{2.7}$$

There are three unknowns in Eq. (2.6), namely e_{13}, e_{11} and $e_{12}e_{14}$. These unknowns can be determined by carrying out measurements on calibration standards, such as open-short-load (OSL), by connecting these standards to the input DUT plane in Fig. 2.6. The measurements on the calibration standard provide a system of three equations (2.8) that relate the error terms and the reflection coefficients, which can be solved to determine the error terms of e_{11}, e_{13} and $e_{12}e_{14}$ [38].

$$\begin{bmatrix} e_{11} \\ e_{13} \\ \Delta e \end{bmatrix} = \begin{bmatrix} 1 & (\Gamma_{in})_{open}(\Gamma_{in}^U)_{open} & -(\Gamma_{in})_{open} \\ 1 & (\Gamma_{in})_{short}(\Gamma_{in}^U)_{short} & -(\Gamma_{in})_{short} \\ 1 & (\Gamma_{in})_{load}(\Gamma_{in}^U)_{load} & -(\Gamma_{in})_{load} \end{bmatrix}^{-1} \begin{bmatrix} (\Gamma_{in}^U)_{open} \\ (\Gamma_{in}^U)_{short} \\ (\Gamma_{in}^U)_{load} \end{bmatrix} \tag{2.8}$$

where $\Delta e = e_{12}e_{14} - e_{11}e_{13}$. Terms Γ_{in} with subscripts open, load and short refer to the actual reflection coefficients of the OSL standards at the DUT plane; whereas terms Γ_{in}^U with subscripts open, load and short are the corresponding measurements at the VNA plane.

The determination of error terms using Eq. (2.8) enables the calibration of the input port for the measurement of an accurate reflection coefficient at the input DUT plane, as given by Eq. (2.7).

For the error model of the output network in Fig. 2.9, e_{26} represents coupling to the power meter, e_{25} denotes directivity errors in the test channel of the network analyzer, and Γ_{2T} and a_{2T} indicate the tuner and node, respectively. This is a general form that can describe any passive or active tuner. A passive tuner has a non-zero Γ_{2T} term and zero a_{2T}, while active tuners have a non-zero a_{2T}. One step in the calibration procedure, which is described in the following paragraphs, requires that a test signal is injected from the right of the output coupler. In this case, a_{2T} is non-zero.

The simplification of signal flow model in Fig. 2.9 gives the error corrected reflection coefficients at the output reference plane, in terms of the uncorrected reading, Γ_L^U, given in Eq. (2.10).

$$\Gamma_L^U = \frac{a_3}{b_3} \tag{2.9}$$

$$\Gamma_L = e_{23} + \frac{e_{22}e_{24}\Gamma_L^U}{1 - e_{21}\Gamma_L^U} \tag{2.10}$$

The simplifications of Figs. 2.8 and 2.9 also provide error corrected input and output power, as per Eqs. (2.11) and (2.12).

$$P_{in} = |P_1|^2 \left|\frac{e_{12}}{e_{16}}\right|^2 \frac{(1 - |\Gamma_{in}|^2)}{|1 - \Gamma_{in}e_{13}|^2} \tag{2.11}$$

$$P_{out} = \frac{|P_2|^2}{|e_{24}e_{26}|^2}|1 - e_{21}\Gamma_L|^2\left(1 - |\Gamma_L|^2\right) \tag{2.12}$$

where $|P_1|^2$ and $|P_2|^2$ are the input and output power meter readings, respectively. It is important to note that the equations are independent of the tuner reflection coefficients, Γ_{1T} and Γ_{2T}, and the directivity terms, e_{15} and e_{25}. Therefore, it is not necessary to obtain explicit values for these four terms.

The measurement of input power requires the determination of the error terms of e_{13}, e_{11} and $e_{12}e_{14}$, which can be obtained by standard one-port VNA calibration techniques in which the DUT is replaced by a series of calibration standards such as a short circuit, an offset short circuit, and an open circuit [39]. The error term $|e_{12}/e_{16}|^2$ in Eq. (2.11) is obtained by connecting a matched power meter in place of the DUT. The ratio of the power meter reading to the input power meter reading is $|e_{12}/e_{16}|^2$.

For the measurement of output power, once again one-port VNA calibration [39] can be performed to determine the error terms e_{21}, e_{23}, and $e_{22}e_{24}$. The input signal for this stage of the calibration, a_{2T}, is injected from the right in Fig. 2.6, with the signal generator and an amplifier connected in place of the load. To determine the error term, $|e_{24}e_{26}|^2$, the magnitude of the insertion loss of the output coupler and power divider, between the DUT output reference plane and the output power meter, is measured. If the test signal injected into the coupler at the DUT reference plane is supplied from a matched source and if the output tuner is replaced by a matched load, the power insertion loss, I_P, is given by:

$$I_P = \frac{|e_{24}e_{26}|^2}{|1 - e_{21}e_{25}|^2} \tag{2.13}$$

Since e_{21} and e_{25} are usually small, the insertion loss measurement gives $|e_{24}e_{26}|^2$ directly.

As a guideline, for maximum accuracy, the system should be calibrated at coaxial (APC-7 or APC-3.5) reference planes close to the test fixture. Then, appropriate de-embedding using coaxial-to-microstrip transition [40] needs to be carried out to transfer the reference plane into the microstrip test fixture.

The available signal power, P_a, at the output of the driver amplifier, in Fig. 2.6 is measured using a matched power meter. The driver amplifier is then connected at the input port of the output directional coupler, in place of the DUT. The corrected output power is obtained for a range of different output tuner settings across the load plane. These power measurements are compared with the calculated output

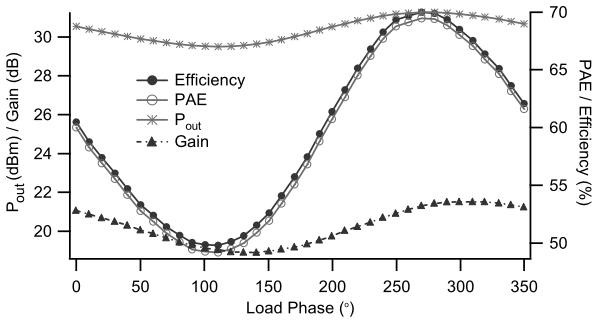

Fig. 2.10 The performance of a 1 W GaAs FET for $|\Gamma_L(2f_0)| = 1$ with a variable phase of the second harmonic, while maintaining optimal fundamental and third harmonic terminations [41], © IOP Journal of Measurement Science and Technology 2010

power, $P_a(1 - |\Gamma_L|^2)$, which is obtained using the measured P_a and the corrected Γ_L. A maximum tolerance of around 0.15 dB between the corrected measured and calculated output power values provides confidence in the calibration process [26].

2.4 Harmonic Load-Pull System

The terminal loading conditions at harmonic frequencies significantly affect device performance. In principle, during the characterization and optimization of transistor devices, the harmonic power generated by the device needs to be fully reflected back at a given phase, in order to extract the best possible efficiency. In an ideal scenario, all the harmonic power can be reflected back; however, this is not possible in practical load-pull systems, due to lossy transition between the tuner and the device. During the characterization of devices, it is a common practice to vary the phase and magnitude of the harmonic reflection coefficients, while keeping the fundamental reflection coefficient constant, in order to obtain optimal efficiency.

Figure 2.10 illustrates an example of the effect of phase variation of $\Gamma_L(2f_0)$ on the performance of a 1 W GaAs (gallium arsenide) FET (field effect transistor) device, while keeping the reflection coefficients at the fundamental frequency and third harmonic fixed [41]. It is apparent that, in this case, the variation of phase of the second harmonic reflection coefficient can swing the efficiency by more than 20 %. Similar effects can be observed when the phase of the third harmonic reflection coefficient or the magnitudes of the second or third harmonic coefficients are varied [42]. Improvements to the tune of over 15 % in efficiency can be achieved in the final designed PA, while terminating the harmonic impedances in optimal terminations, compared to 50 Ω [43]. In addition to the harmonically tuned PAs, the harmonic terminations play a key role in the design of switching-mode PAs [44].

Device characterization for the optimal design of either harmonically tuned PAs or switching-mode PAs is carried out using a harmonic load-pull system [45–47]. One of the first reported passive harmonic load-pull setups [33], which is shown in Fig. 2.11, was based around a circulator. The architecture used standard slide screw tuners, filters and power meters to monitor and control the magnitude and phase of the reflected signal components at the fundamental and second harmonic frequencies. This setup, although very basic when compared to current developments, did

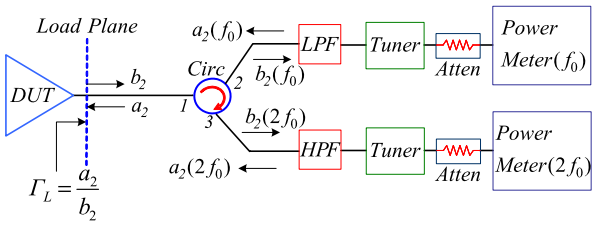

Fig. 2.11 This architecture was one of the first passive harmonic load-pull setups [33], © IEEE 1979

achieve tuning of impedances for fundamental and second harmonic frequencies. In this setup, the transmitted wave, b_2, enters the circulator via port 1; and, the fundamental and second harmonic components exit through the appropriate low-pass and high-pass filters at ports 2 and 3, respectively. The respective tuners reflect the traveling waves, $a_2(f_0)$ and $a_2(2f_0)$, and subsequently synthesize the respective fundamental and second harmonic reflection factors at the load plane given by Eqs. (2.14) and (2.15).

$$\Gamma_L(f_0) = \frac{a_2(f_0)}{b_2(f_0)} \tag{2.14}$$

$$\Gamma_L(2f_0) = \frac{a_2(2f_0)}{b_2(2f_0)} \tag{2.15}$$

The reflected traveling waves, $a_2(f_0) = \Gamma_L(f_0)b_2(f_0)$ and $a_2(2f_0) = \Gamma_L(2f_0) \times b_2(2f_0)$, then combine at port 1 of the circulator to form the overall reflected traveling wave, a_2, as given in Eq. (2.16):

$$a_2 = a_2(f_0) + a_2(2f_0) = \Gamma_L(f_0)b_2(f_0) + \Gamma_L(2f_0)b_2(2f_0) \tag{2.16}$$

In theory, an n-port wideband circulator with appropriate band-pass filters can be employed to extend this setup to $n-1$ harmonics. However, in practice, it is not feasible, considering the bandwidth limitation and substantial losses associated with circulators beyond the second harmonic. Usually, high harmonic reflection coefficients are required, and the losses render the circulator based harmonic load-pull system inappropriate in practical applications. In addition, the poor isolation of circulators also affects the system's ability to synthesize harmonically independent reflection coefficients and, therefore, limits the overall usefulness of this harmonic load-pull setup.

Over the years, passive harmonic load-pull architectures and setups have evolved to address the two major issues of high reflection factor synthesis at harmonic frequencies and harmonically independent reflection factor emulation [17, 18]. These developments in the harmonic load-pull architectures can be grouped in three distinct categories, namely triplexer based harmonic load-pull, harmonic rejection tuner harmonic load-pull and multipurpose single tuner harmonic load-pull [17].

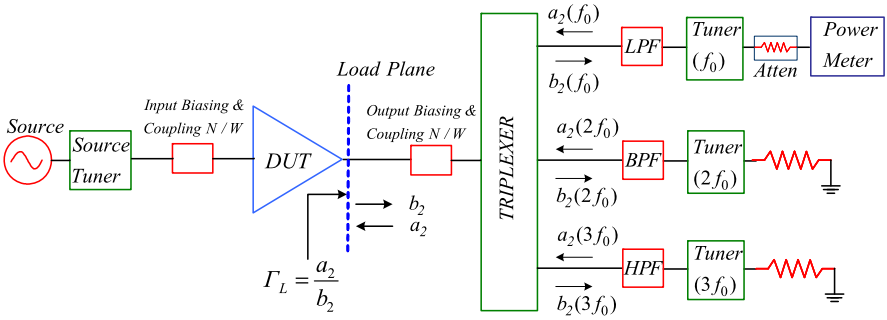

Fig. 2.12 Block diagram of triplexer based three-harmonic load-pull system

2.4.1 Triplexer Based Harmonic Load-Pull Setup

A block diagram of a typical three-harmonic triplexer based load-pull architecture is shown in Fig. 2.12. It is apparent that an appropriate triplexer and tuners corresponding to carrier and harmonic frequencies are required to build a triplexer based harmonic load-pull system. The input and output biasing networks provide for the biasing at the gate and source, respectively and, the input and output coupling networks are needed for capturing the transmitted and reflected traveling waves at the input and output ports, respectively. The optional source tuner is used for matching at the input port. The triplexer, which acts like filters for the respective harmonic components, separates the harmonic components from the output generated by the DUT. The subsequent filters at the output of the triplexer further improve the rejection of the out-of-band frequency components.

The respective load-tuners for harmonic components f_0, $2f_0$, and $3f_0$ tune the reflection environment as per specific requirements and reflect the respective $a_2(f_0)$, $a_2(2f_0)$, and $a_2(3f_0)$ and, in the process, synthesize the harmonically independent reflection factors by interacting with the respective components, $b_2(f_0)$, $b_2(2f_0)$ and $b_2(3f_0)$, of the traveling wave, b_2. The reflected traveling wave components, having different weighting factors, contributed by the tuners, then combine to form the overall a_2 given in Eq. (2.17).

$$a_2 = a_2(f_0) + a_2(2f_0) + a_2(3f_0) \tag{2.17}$$

The primary benefit of such a technique is that the reflection factors at different harmonic frequencies can be set independently, i.e., the harmonic reflection factors are independent of each other. It can thus be inferred that this method gives full magnitude and phase control of all three harmonic frequencies, f_0, $2f_0$, and $3f_0$. The drawback of this technique is the limited tuning coverage at the harmonics, as shown in Fig. 2.13, due to the losses inherent in the triplexer. This is a serious limitation for applications requiring high harmonic terminations, such as class-F and inverse class-F mode PAs [48].

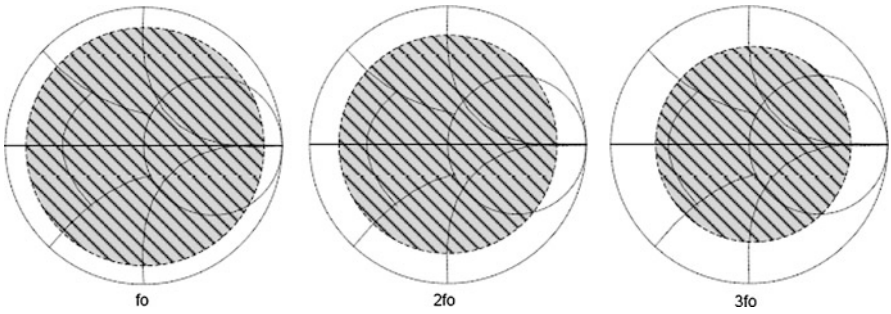

Fig. 2.13 Depiction of tuning coverage at f_0, $2f_0$ and $3f_0$ for the triplexer based three-harmonic load-pull system [17]

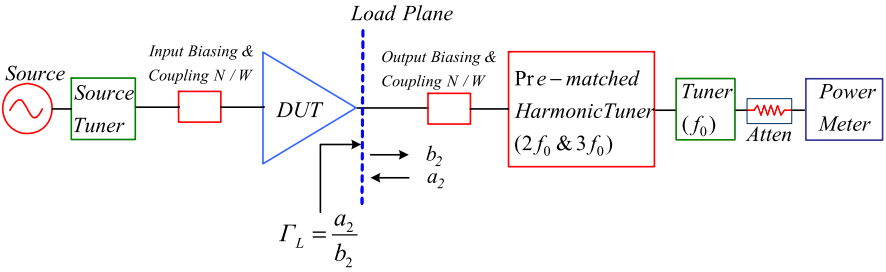

Fig. 2.14 The harmonic rejection tuner based three-harmonic load-pull architecture

2.4.2 Harmonic Rejection Tuner Based Harmonic Load-Pull Setup

The harmonic rejection tuner (HRT) based harmonic load-pull architecture incorporates an HRT in addition to a fundamental tuner, as shown in Fig. 2.14. In a standard HRT based harmonic load-pull setup, pre-matched type harmonic tuners, as explained in Chap. 5, such as passive harmonic tuners (PHT) [17] are used.

The fundamental tuner, possessing full magnitude and phase control for the reflection coefficient at the fundamental frequency, f_0, is placed farther from the DUT output port, as the reflection coefficient required at the fundamental frequency is smaller than those of the harmonic frequencies. The HRT, which is capable of full phase control at harmonic frequencies $2f_0$ and $3f_0$, is placed nearer to the DUT port, in order to minimize the impact of the loss associated with the cables and connectors. This helps in the synthesis of higher reflection coefficients at the harmonic frequencies.

Furthermore, this technique overcomes the loss associated with the triplexer; therefore. the reflection coefficient can cover a larger region on the Smith chart, as shown in Fig. 2.15. The harmonic rejection tuners are low loss, which also contributes to the synthesis of reflection coefficient with increased magnitude. It is also evident that the HRTs, although are capable of providing higher reflection coefficients, do preclude a large portion of Smith chart. This limitation, however, does not

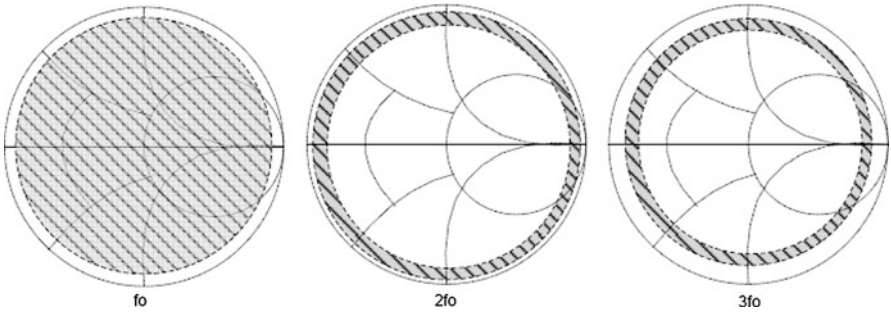

Fig. 2.15 Depiction of tuning coverage at f_0, $2f_0$ and $3f_0$ for the HRT based three-harmonic load-pull system [17]

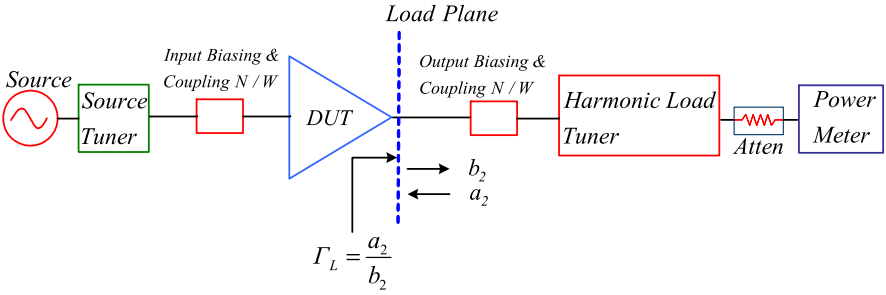

Fig. 2.16 The multipurpose tuner based harmonic load-pull architecture

affect the usefulness in practical applications considering that the required harmonic reflection coefficients usually fall nearer the boundary of the Smith chart.

The primary limitation of this technique is the poor isolation between the synthesized reflection coefficients at the fundamental and harmonic frequencies. This is due to the fact that the tuners are cascaded; therefore, setting of the tuner state at one frequency affects the tuner state at the other frequencies. As a consequence, this technique becomes impractical for more than three harmonic frequencies.

2.4.3 Single Tuner Harmonic Load-Pull Setup

Figure 2.16 shows a typical block diagram of a single tuner harmonic load-pull setup, which also includes a source tuner and peripheral biasing and measuring network. In this architecture, a multipurpose load tuner that covers the fundamental frequency and the range of all of the relevant harmonic frequencies is employed for the synthesis of harmonically independent fundamental and harmonic reflection coefficients [17].

For example, a three-harmonic multipurpose tuner uses three independent wideband probes for the control of the magnitude and phase of the reflection coefficients

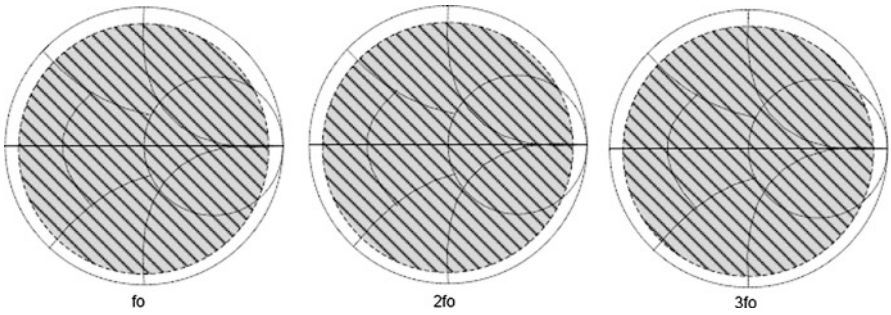

Fig. 2.17 Depiction of tuning coverage at f_0, $2f_0$ and $3f_0$ for the single multipurpose tuner based three-harmonic load-pull system [17]

at the three harmonic frequencies of f_0, $2f_0$, and $3f_0$. The proper positioning and movement of the three probes in the horizontal and vertical directions allow independent tuning at the three harmonic frequencies [17]. A multipurpose tuner gives full magnitude and phase control for all three harmonic frequencies, as shown in Fig. 2.17.

Since this setup utilizes only one tuner, the overall system loss associated with biasing and measuring networks, cables and connectors is less; hence, the achievable magnitude of the reflection coefficient is higher than other harmonic load-pull architectures. This setup is compact and smaller in size compared to the types of other setups. A major limitation of this technique includes the requirement for very powerful computing facility to monitor and control the movement of the tuner probes. In addition, this technique also suffers from inherent limited isolation, due to the series configuration of all the probes. The limited isolation prevents this setup from synthesizing harmonically independent harmonic reflection coefficients at all frequencies and in all parts of the Smith chart.

2.4.4 Harmonic Load-Pull Comparisons

The harmonic tuning methods can be compared primarily in two aspects, namely the tuning isolation and the effective Smith chart coverage.

An important factor of any load-pull device characterization system is the accuracy at which the impedance seen by the DUT at the fundamental frequency can be controlled. If the impedance changes without the user's knowledge or if it cannot be kept constant for varying harmonic impedances, the measurement results obtained are invalid. Hence, when considering harmonic load-pull systems, it is essential to know the isolation across frequencies.

The triplexer based harmonic load-pull architecture relies on the isolation inherent within the isolator to mitigate the effects of variation in the setting of one tuner from setting of another. Triplexers typically possess 50–60 dB of isolation at the fundamental and harmonic frequencies; therefore, this technique can practically

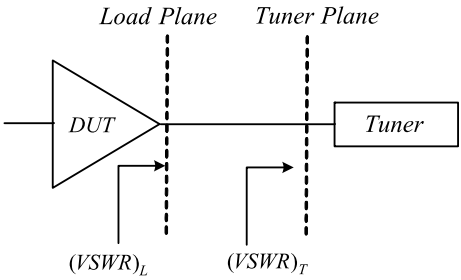

Fig. 2.18 Definition of VSWR at load and tuner planes for a fundamental load-pull tuning setup

tune harmonic impedances independent of each other. In some applications, poor isolation outside the fundamental and harmonic frequency band can cause spurious oscillations, especially at low frequencies, due to high out-of-band reflections.

In the HRT based harmonic load-pull setup, the frequency isolation between the harmonic resonators is around 30 dB. The poor frequency isolation is the result of the sum of vectors generated by the reflections at f_0, $2f_0$, and $3f_0$, as well as the residual reflection of the slab-line [17]. This makes setting of harmonically independent impedances extremely difficult.

In the case of the multipurpose tuner, the fundamental and harmonic probes reposition themselves for each desired reflection factor for the combination of f_0, $2f_0$, and $3f_0$, which helps in achieving very good tuning isolation. However, the measurement using multipurpose based harmonic load-pull is relatively slow, due to physical movement of probes for each set of harmonic impedances.

For tuning range, it is the effective voltage standing wave ratio (VSWR) at the load plane that matters and not the tuner's ability to synthesize the VSWR at the tuner plane. The VSWR at the load plane depends on the interface between the tuner and the DUT and gets reduced accordingly. Figure 2.18 provides a simple relationship of the VSWR at the load and tuner planes. It is important to note that there are always a passive measurement network and transition between the DUT and the tuner, which reduce the achievable VSWR at the load plane compared to the tuner plane.

In a triplexer based harmonic load-pull setup, as shown in Fig. 2.12, there is loss due to the insertion loss of the triplexer, which is responsible for the reduced Smith charge coverage shown in Fig. 2.13. The coverage gets further reduced at harmonic frequencies, as the triplexer loss at harmonic frequencies is higher.

In the case of HRT based harmonic load-pull architecture, there are only measuring passive networks between the tuner and the DUT, as shown in Fig. 2.14; therefore, the reduction in the Smith chart coverage is smaller. However, there is a transition between the fundamental and harmonic tuners, causing reduction in the VSWR and further reducing the Smith chart coverage at the fundamental frequency, f_0, as shown in Fig. 2.15, compared to the harmonic frequencies.

In a single multipurpose tuner, the reduction in the VSWR at the harmonic and fundamental frequencies is almost similar, as all the tuning probes are contained in a single casing. The reductions in the VSWR at the fundamental and harmonic frequencies are caused only by the passive measuring network between the tuner and the DUT.

Table 2.2 Features of harmonic tuning methods [17]

Tuning method	Advantages	Disadvantages
Triplexer based	– High tuning isolation	– Unsuitable for on-wafer applications
	– Simple extension of existing setup	– Insertion loss of the triplexer at all frequencies causes a reduced tuning range
	– Very good amplitude and phase control at all the harmonic frequencies	– Out-of-band reflections in the triplexer can cause spurious oscillations
Harmonic rejection tuner based	– High tuning range	– Very poor tuning isolation
	– High power handling capability	– Unsuitable for broadband applications
	– Low insertion loss at fundamental frequency	– Limited to only three harmonics
Multipurpose single tuner based	– High tuning range	– Slow measurement time and throughput
	– High tuning isolation	– Requires powerful computing resource
	– Ideal for on-wafer applications	
	– Appropriate for broadband applications	

Table 2.2 summarizes the major features of the described three different harmonic load-pull techniques.

2.5 Tuning Range Enhancement

The tuning range in a passive load-pull system is limited, due to the inherent losses in the biasing and measuring network, connectors, cables, fixture and the tuner itself [30]. Therefore, depending on the load-pull system architecture, a substantial part of the Smith chart is precluded; and, as a consequence, not all relevant impedances can be synthesized

Most of the low-power device characterization and PA design requirements are met by standard passive load-pull setups. However, limitations of such systems are apparent during high-power device characterization and PA design or harmonic load-pull measurements, as these situations require highly reflective impedance environments. To address this issue, several solutions have been proposed [12].

The enhanced loop [49] and cascaded tuner architectures [18] are recent developments in passive load-pull architectures that have the ability to synthesize high reflection coefficients. In both of these systems, the idea is the enhancement of the

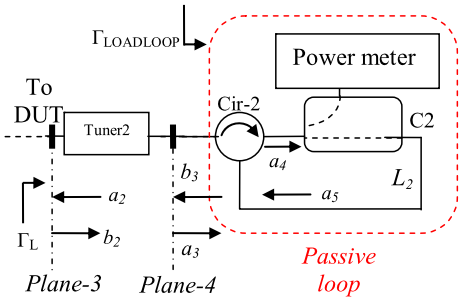

Fig. 2.19 The enhanced loop load-pull architecture for synthesizing a high reflection coefficient [49], © IEEE 2010

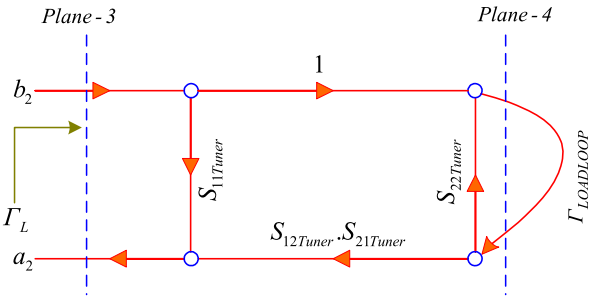

Fig. 2.20 The signal flow model depicting the generation of reflection factor using enhanced loop load-pull architecture [49], © IEEE 2010

tuning range by reflecting back the transmitted signal that is transmitted through the main tuner.

2.5.1 Enhanced Loop Architecture

In order to achieve high reflection factors, this technique combines a passive tuner and a passive loop, as shown in Fig. 2.19. It employs a low-loss circulator, *Cir-2*, with very high directivity, so that the loss incurred in the setup is smaller and that there is good isolation between signals a_4 and b_3. The employed coupler, *C2*, and the loop cable, L_2, are low loss. The coupling port of the coupler is connected to a power meter, in order to monitor and measure the DUT performances, in terms of output power or linearity, during load-pull characterization. The passive loop at the output of Tuner2 generates reflection coefficient $\Gamma_{LOADLOOP}$ at *plane-4* and augments the overall reflection coefficient Γ_L at *plane-3*. The flow model in Fig. 2.20 depicts the generation of reflection factor Γ_L at *plane-3*.

The following expressions relate the traveling waves in the enhanced loop load-pull architecture of Fig. 2.19:

$$a_4 = k_4 a_3 \tag{2.18}$$

$$a_5 = k_5 a_4 \tag{2.19}$$

$$b_3 = k_6 a_5 \tag{2.20}$$

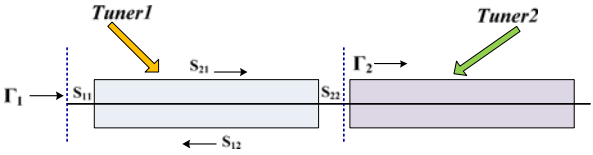

Fig. 2.21 Two tuners cascaded in series to obtain higher reflection factor [18], © Maury Microwave Corporation

where k_4, k_5 and k_6 are the complex factors dependent on the S-parameters of the circulator, *Cir-2*, and the directional coupler, *C2*.

The mismatch between *Tuner2* and the passive loop plane, *Plane-4*, is related by the following expression:

$$\Gamma_{LOADLOOP} = K_L = \frac{b_3}{a_3} = |K_L| e^{-2j\beta L_2} \tag{2.21}$$

where the parameter $K_L (= k_4 k_5 k_6)$ is a complex factor that depends on the passive loop structure characteristics, i.e., the transmission factors of coupler *C2* and circulator *Cir-2*.

It is clear from Eq. (2.21) that the reflection coefficient generated by the passive loop is also dependent on the phase velocity, β, of the traveling waves and the length of cable in the passive loop, L_2. The simplification of the flow model in Fig. 2.20 results in the following expression for the overall reflection coefficient at *plane-3*.

$$\Gamma_L = \frac{b_2}{a_2} = S_{11TUNER2} + \frac{S_{12TUNER2} S_{21TUNER2} K_L}{1 - S_{22TUNER2} K_L} \tag{2.22}$$

Equation (2.16) demonstrates that the total load reflection coefficient, Γ_L, at *plane-3* gets enhanced by the contribution from the passive loop. If the loop does not contribute anything to the overall reflection coefficient, then S_{11} of *Tuner2* is the total reflection coefficient.

2.5.2 Cascaded Tuner

Figure 2.21 depicts the cascading of two passive tuners in series. The cascaded tuners are capable of generating reflection factor, Γ_1, at the DUT plane, which is governed by Eq. (2.23) [18].

$$\Gamma_1 = S_{11} + \frac{S_{12} S_{21} \Gamma_2}{1 - S_{22} \Gamma_2} \tag{2.23}$$

where S_{11}, S_{21}, S_{12}, and S_{22} are the S-parameters of *Tuner1* (closest to the DUT). Γ_2 is S_{11} looking into *Tuner2* at a particular termination.

The overall reflection looking into the cascaded tuner combination is equal to the complex reflection of the first tuner added to the complex reflection of the second tuner and multiplied by some insertion/reflection factor. It is important to notice that the effect of the second tuner is highly influenced by the $S_{21} S_{12}$ product of the first tuner. There are two extreme cases that best describe this effect [18]:

- If *Tuner1* is at a physical short circuit, i.e., $S_{21}S_{12} = 0$, *Tuner2* would be completely masked.
- If *Tuner1* is at initialized at 50 Ω, i.e., $S_{11} \sim 0$ and $S_{21}S_{12} \sim 1$, *Tuner2* would be all that is seen.

References

1. J.M. Cusack, S.M. Perlow, B.S. Perlman, Automatic load contour mapping for microwave power transistors. IEEE Trans. Microw. Theory Tech. **22**, 1146–1152 (1974)
2. F. Secchi, R. Paglione, B. Perlman, J. Brown, A computer controlled microwave tuner for automated load pull. RCA Rev. **44**(4), 566–583 (1983)
3. Focus Microwave, Mechanical vibrations of CCMT tuners used in on-wafer load-pull testing, Application Note AN-46, Oct. 2001
4. J. Sevic, Introduction to tuner-based measurement and characterization, Technical Note, Maury Microwave Corporation, 5C-054
5. D.M. Pozar, *Microwave Engineering*, 3rd edn. (Wiley, New York, 2005). ISBN 0-471-17096-8
6. Microlab, Mechanical tuners, Application Note, Oct. 2000
7. R. Tuijtelaars, Overview of device noise parameter measurement system, in *VDE/ITG-23.10.01* (2001), pp. 1–5
8. Maury Microwave Corporation, Device characterization with harmonic load and source pull, Application Note: 5C-044, Dec. 2000
9. Focus Microwave, Load pull measurements on transistors with harmonic impedance control, Technical Note, Aug. 1999
10. B.W. Leake, A programmable load for power and noise characterization, in *IEEE Microwave Theory and Techniques Society's International Microwave Symposium Digest*, Dallas, USA (June 1982), pp. 348–350
11. Maury Microwave Corporation, LP series electronic tuner system, Technical Data, 4T-081, 2002
12. M.S. Hashmi, F.M. Ghannouchi, P.J. Tasker, K. Rawat, Highly reflective load-pull. IEEE Microw. Mag. **11**(4), 96–107 (2011)
13. Focus Microwave, Computer controlled microwave tuner—CCMT, Product Note 41, Jan. 1998
14. Maury Microwave Corporation, Slide screw tuners, Technical Data, 2G-035A, Feb. 1998
15. Focus Microwaves, Algorithms for automatic high precision residual tuning to 50 Ω using programmable tuners, Application Note 45, May 2001
16. Focus Microwave, Electronic tuners (ETS) and electromechanical tuners (EMT)—a critical comparison, Technical Note, Aug. 1998
17. Focus Microwave, Comparing harmonic load-pull techniques with regards to power-added efficiency (PAE), Application Note 58, May 2007
18. Maury Microwave Corporatio, Cascading tuners for high-VSWR and harmonic applications, Application Note 5C-081, Jan. 2009
19. F. Deshours, E. Bergeault, F. Blache, J.-P. Villotte, B. Villeforceix, Experimental comparison of load-pull measurement systems for nonlinear power transistor characterization. IEEE Trans. Instrum. Meas. **57**(11), 1251–1255 (1997)
20. A. Ferrero, V. Teppati, Experimental comparison of active and passive load-pull measurement technologies, in *30th European Microwave Conference Proceedings*, Paris, France (Oct. 2000), pp. 1–4
21. C. Arnaud, J.L. Carbonero, J.M. Nebus, J.P. Teyssier, Comparison of active and passive load-pull test benches, in *57th ARFTG Conference*, vol. 39 (May 2001), pp. 1–4

22. M.S. Hashmi, A.L. Clarke, S.P. Woodington, J. Lees, J. Benedikt, P.J. Tasker, An accurate calibrate-able multiharmonic active load-pull system based on the envelope load-pull concept. IEEE Trans. Microw. Theory Tech. **58**(3), 656–664 (2010)
23. W.S. El-Deeb, N. Boulejfen, F.M. Ghannouchi, A multiport measurement system for complex distortion measurements of nonlinear microwave systems. IEEE Trans. Instrum. Meas. **59**(5), 1406–1413 (2010)
24. D. Barataud, F. Blache, A. Mallet, P. Bouysse, J.-M. Nebus, J. Villotte, J. Obregon, J. Verspecht, P. Auxemery, Measurement and control of current/voltage waveforms of microwave transistors using a harmonic load-pull system for the optimum design of high efficiency power amplifiers. IEEE Trans. Instrum. Meas. **48**(4), 835–842 (1999)
25. J.E. Mueller, B. Gyselinckx, Comparison of active versus passive on-wafer load-pull characterization of microwave MMwave power devices, in *IEEE Microwave Theory and Techniques Society's International Microwave Symposium Digest*, San Diego, USA (June 1994), pp. 1077–1080
26. R.S. Tucker, P.D. Bradley, Computer-aided error correction of large-signal load-pull measurements. IEEE Trans. Microw. Theory Tech. **32**(3), 296–300 (1984)
27. P.D. Bradley, R.S. Tucker, Computer-corrected load-pull characterization of power MESFETs, in *IEEE Microwave Theory and Techniques Society's International Microwave Symposium Digest*, Boston, USA (June 1983), pp. 224–226
28. C. Tsironis, Adaptable pre-matched tuner system and method, US Patent No. 6674293
29. G.R. Simpson, Impedance tuner systems and probes, US Patent No. 7589601
30. J. Sirois, B. Noori, Tuning range analysis of load-pull measurement systems and impedance transforming networks, in *69th ARFTG Conference*, Honolulu, USA (June 2007), pp. 1–5
31. C. Roff, J. Graham, J. Sirois, B. Noori, A new technique for decreasing the characterization time of passive load-pull tuners to maximize measurement throughput, in *72nd ARFTG Conference*, Portland, USA (Dec. 2008), pp. 92–96
32. P. Hart, J. Wood, B. Noori, P. Aaen, Improving loadpull measurement time by intelligent measurement interpolation and surface modeling techniques, in *67th ARFTG Conference*, San Francisco, USA (June 2006), pp. 69–72
33. R.B. Stancliff, D.B. Poulin, Harmonic load-pull, in *IEEE Microwave Theory and Techniques Society's International Microwave Symposium Digest*, Florida, USA (Apr. 1979), pp. 185–187
34. E.W. Strid, Measurement of losses in noise-matching networks. IEEE Trans. Microw. Theory Tech. **29**(3), 247–252 (1981)
35. G.P. Bava, U. Pisani, V. Pozzolo, Active load technique for load-pull characterization at microwave frequencies. IEE Electron. Lett. **18**(4), 178–180 (1982)
36. Y. Takayama, A new load pull characterization method for microwave power transistors, in *IEEE Microwave Theory and Techniques Society's International Microwave Symposium Digest*, New Jersey, USA (June 1976), pp. 218–220
37. R.A. Hackborn, An automatic network analyzer system. Microw. J. **May**, 45–52 (1968)
38. W.S. El-Deeb, M.S. Hashmi, S. Bensmida, N. Boulejfen, F.M. Ghannouchi, Thru-less calibration algorithm and measurement system for on-wafer large-signal characterization of microwave devices, IET J. Microw. Antenna Propag. **4**(11), 1773–1781 (2010)
39. E.F. DaSilva, M.K. McPhun, Calibration technique for one-port measurements. Microw. J. **June**, 97–100 (1978)
40. J.R. Souza, E.C. Talboys, S-parameter characterization of coaxial to microstrip transition. IEE Proc. **129**(Part H), 37–40 (1982)
41. M.S. Hashmi, A.L. Clarke, J. Lees, M. Helaoui, P.J. Tasker, F.M. Ghannouchi, Agile harmonic envelope load-pull system enabling reliable and rapid device characterization. IOP J. Meas. Sci. Technol. **21**(055109), 1–9 (2010)
42. M.S. Hashmi, A.L. Clarke, S.P. Woodington, J. Lees, J. Benedikt, P.J. Tasker, Electronic multiharmonic load-pull system for experimentally driven power amplifier design optimization, in *IEEE Microwave Theory and Techniques Society's International Microwave Symposium Digest*, Boston, USA, vols. 1–3 (June 2009), pp. 1549–1552

43. F. Blache, J.-M. Nebus, P. Bouysse, L. Jallet, A novel computerized multiharmonic active load-pull system for the optimization of high-efficiency operating classes in power transistor, in *IEEE International Microwave Symposium Digest*, Orlando, USA (June 1995), pp. 1037–1040
44. A. Grebennikov, N.O. Sokal, *Switch Mode RF Power Amplifiers* (Elsevier, Oxford, 2007)
45. F.M. Ghannouchi, F. Beauregard, A.B. Kouki, Power added efficiency and gain improvement in MESFETs amplifiers using an active harmonic loading technique. Microw. Opt. Technol. Lett. **7**(13), 625–627 (1994)
46. R. Hajji, F.M. Ghannouchi, R.G. Bosisio, Large-signal microwave transistor modeling using multiharmonic load-pull measurements. Microw. Opt. Technol. Lett. **5**(11), 580–585 (1992)
47. F.M. Ghannouchi, R. Larose, R.G. Bosisio, A new multiharmonic loading method for large-signal microwave and millimeter-wave transistor characterization. IEEE Trans. Microw. Theory Tech. **39**(6), 986–992 (1991)
48. Y.Y. Woo, Y. Yang, B. Kim, Analysis and experiments for high efficiency class-F and inverse class-F power amplifiers. IEEE Trans. Microw. Theory Tech. **54**(5), 1969–1974 (2006)
49. F.M. Ghannouchi, M.S. Hashmi, S. Bensmida, M. Helaoui, Enhanced loop passive source- and load-pull architecture for high reflection factor synthesis. IEEE Trans. Microw. Theory Tech. **58**(11), 2952–2959 (2010)

http://www.springer.com/978-94-007-4460-8

Load-Pull Techniques with Applications to Power Amplifier Design

Ghannouchi, F.M.; Hashmi, M.S.

2013, XIV, 234 p., Hardcover
ISBN: 978-94-007-4460-8